3D visualisation of voids in grapevine flowers and berries using X-ray micro computed tomography

Z. XIAO[1,2,3], T. STAIT-GARDNER[3], S.A. WILLIS[3], W.S. PRICE[3], F.J. MORONI[2], V. PAGAY[1,4], S.D. TYERMAN[1,4], L.M. SCHMIDTKE[1,2] and S.Y. ROGIERS[1,2,3,5]

[1] Australian Research Council Training Centre for Innovative Wine Production, The University of Adelaide, Glen Osmond, SA, 5064, Australia; [2] National Wine and Grape Industry Centre, Charles Sturt University, Wagga Wagga, NSW, 2678, Australia; [3] Nanoscale Organisation and Dynamics Group, Western Sydney University, Penrith, NSW, 2751, Australia; [4] Department of Wine Science and Waite Research Institute, The University of Adelaide, Glen Osmond, SA, 5064, Australia; [5] NSW Department of Primary Industries, Wollongbar Primary Industries Research Institute, Wollongbar, NSW, 2477, Australia

Corresponding author: Dr Suzy Rogiers, email suzy.rogiers@dpi.nsw.gov.au

Abstract

Background and Aim: X-ray micro computed tomography (micro-CT) is a non-destructive 3D imaging technique that has been applied to plant morphology and anatomical studies to gain a better understanding of physiological phenomena in vivo. It is particularly useful for imaging voids in undisturbed fragile tissues and therefore may be applied to the delicate flowers and soft berries of *Vitis vinifera*. The characterisation of gas spaces and channels can offer insights into the process of tissue aeration and this may have implications on cell function and vitality. We assessed the use of micro-CT to visualise voids within these reproductive organs.

Methods and Results: The internal structures of flowers and berries were captured through rapid micro-CT scanning and subsequently were recreated in 3D using image processing. The relative positions of the developing flower parts encased within the flower cap were visualised. Low density/porous tissue was identified within the pedicel and receptacle, connecting the lenticels with the interior of the berry. Voids were present in the proximal mesocarp of mature berries forming a 'detachment zone' in both seeded and seedless cultivars. Voids permeated the mesocarp of mature seedless grape cultivars, but not seeded grapes.

Conclusion: Micro-CT offers new insights regarding the distribution of voids on the morphology and compositional heterogeneity of organs that are difficult to dissect and/or view with light microscopy.

Significance of the Study: A better understanding of the physiology and functionality of grapevine reproductive tissues may be achieved by 3D visualisation of internal structure in vivo.

Keywords: *3D visualisation, flower, grape morphology, micro-CT,* Vitis vinifera

Introduction

3D X-ray micro computed tomography (micro-CT) imaging of plant components began in the late 1990s (Heeraman et al. 1997) and has been expanding rapidly since. Micro-CT has been applied to plants for visualising whole organ structure (Wang et al. 2015), undisturbed root architecture (Tracy et al. 2010), seed composition (Gargiulo et al. 2019), inflorescence architecture (Li et al. 2019), vascular tissue anatomy (Brodersen et al. 2011, Wason et al. 2017), xylem embolism (Cochard et al. 2015), mineral and crystal deposition (Pierantoni et al. 2017), cell volume (Herremans et al. 2015), tissue porosity (Verboven et al. 2015, Xiao et al. 2018b, Signorelli et al. 2020) and insect pest invasion (Alba-Alejandre et al. 2018). Generally, an X-ray source is rotated around the specimen and the numerous shadow images on a rotating X-ray detector at different angles can be reconstructed into a 3D data set made up of voxels (i.e. projection reconstruction). Anatomical features can be revealed in the 3D data set if there are differences in the density and atomic mass of the material the voxel represents, which is related to the brightness of the voxels (du Plessis and Broeckhoven 2019).

Prior to micro-CT and other 3D imaging techniques, such as positron emission tomography (PET) (Hubeau and Steppe 2015) and magnetic resonance imaging (MRI) (Dean et al. 2014, 2016), only destructive sampling and time-consuming classical histology was available to examine internal structures of plants. This can be challenging for soft and easily damaged tissues such as ripe berries where specimens require sectioning into small samples to assess internal features. Furthermore, the fixation, embedding and staining procedure can result in artefacts. Micro-CT is a preferred option because overall morphology, surface features and internal structures can be visualised rapidly and non-destructively and is not constrained by two dimensions. Depending on the X-ray source, the achievable resolution of a 3D micro-CT reconstruction is of the order of several micrometres. Unlike confocal microscopy, thickness and transparency of the sample does not limit optical depth. The addition of contrast agents composing of heavy metals such as caesium can provide further contrast enhancement (Staedler et al. 2013, Wang et al. 2017) but depending on the application little or no sample preparation may be required. A further advantage of micro-CT is the ability to

doi: 10.1111/ajgw.12480

carry out repetitive imaging to gain a better understanding of time-dependent changes in vivo (Brodersen et al. 2013, Knipfer et al. 2015a).

Flower and fruit development are the most critical stages in grapevine development as they determine yield and grape composition, and the anatomical and morphological aspects of berry development have been comprehensively described (Pratt 1971, Hardie et al. 1996, May 2000). Although scanning electron microscopy has provided much detail on grapevine inflorescence and flower development (Srinivasan and Mullins 1981, Boss et al. 2003, Shavrukov et al. 2004), it does not allow visualisation of the internal structures. The development of the male and female flower parts are obscured by the 'cap', the corolla of interlocked petals (Srinivasan and Mullins 1976) and the relatively limited information on gynoecium development, as highlighted by Boss et al. (2003), can potentially be enhanced with micro-CT.

Grape berries undergo colour change, rapid sugar accumulation and softening during ripening (Kuhn et al. 2013). Tissue aeration is critical for normal metabolic processes, however, berries are covered with a thick waxy cuticle and lenticels on the berry skin are occluded (Rogiers et al. 2004, 2005). In a previous study we suggested that oxygen may diffuse into the berry through the lenticels on the pedicel and demonstrated that when these structures were covered with an impermeable gel, tissue oxygen concentration declined (Xiao et al. 2018b). In that study, a diffuse porous gas network distributed through the intracellular spaces of the berry mesocarp was revealed using micro-CT. The fate of these voids is still unclear. They may become saturated with cellular fluid and/or, instead, larger voids may form due to tissue collapse as cell walls break down during ripening (Nunan et al. 1998). The characterisation of fine and macroscopic voids within fruit has important implications for understanding cell vitality and senescence processes pre- and postharvest (Herremans et al. 2015, Xiao et al. 2018b).

Accordingly, the main aim of this study was to provide information on the occurrence and distribution of voids in developing grape reproductive organs, including inflorescences, flowers and berries, in vivo by using micro-CT.

Materials and methods

Plant material

Inflorescences of Isabella (*V. vinifera* × *V. labrusca*) and Schwarzmann (*V. riparia* × *V. rupestris*) and berries of *V. vinifera* L. cultivars Shiraz, Merlot, Sémillon, Cabernet Sauvignon, Sultana, Flame Seedless, Muscat Gordo Blanco, Nyora and the hybrids Isabella and Chambourcin (Joannes Seyve 11369 × Plantet) were sampled from grapevines grown in the experimental vineyard at the National Wine and Grape Industry in Wagga Wagga, NSW (35°3′38.57″S; 147°21′42.89″E; 121 masl). The 14-year-old vines were own-rooted, carried approximately 30 shoots per vine in a sprawling canopy on a two-wire vertical trellis and were irrigated to maintain a volumetric soil water content of approximately 20% during ripening.

Inflorescences were sampled on the same day (approximately 12–22 days prior to 80% cap-fall depending on cultivar) and berries were sampled approximately 3 months later [92–102 days after flowering (DAF) depending on the cultivar], also on the same day. Four replicate samples, each comprising ten inflorescences/berries from three vines, were collected, from a randomised block with each cultivar (i.e. in three-vine panels) replicated in four different rows. They were immediately placed into plastic containers and transported on ice to the Biomedical Magnetic Resonance Facility at Western Sydney University, a node of the National Imaging Facility, where they were imaged within 48 h. For each cultivar, a subsample of four berries, one from each replicate, was used for imaging. Presence of voids in berry parts was surveyed from all four berries imaged, while total void volume and void volume (%) (below) were calculated only for berries presented as whole in the micro-CT final data sets. Another subsample of four berries was used for measurement of TSS using a ATAGO PAL-1 digital hand-held refractometer (ATAGO, Tokyo, Japan). Firmness was assessed subjectively by sight and categorised as either turgid or shrivelled.

Micro-CT imaging and image processing

A Quantum GX micro-CT (PerkinElmer, Waltham, MA, USA) was used for imaging. The inflorescences and berries were imaged intact within plastic containers so as to prevent dehydration. Specimens were scanned with a beam voltage of 90 kV and current of 88 μA in 14 min. The Quantum GX was used for reconstructing 2D projections into stacks of DICOM file, with a pixel resolution of 50 μm or 1.25×10^{-4} mm^3 voxel size. Berry greyscale slices were generated using Volume Viewer plugin

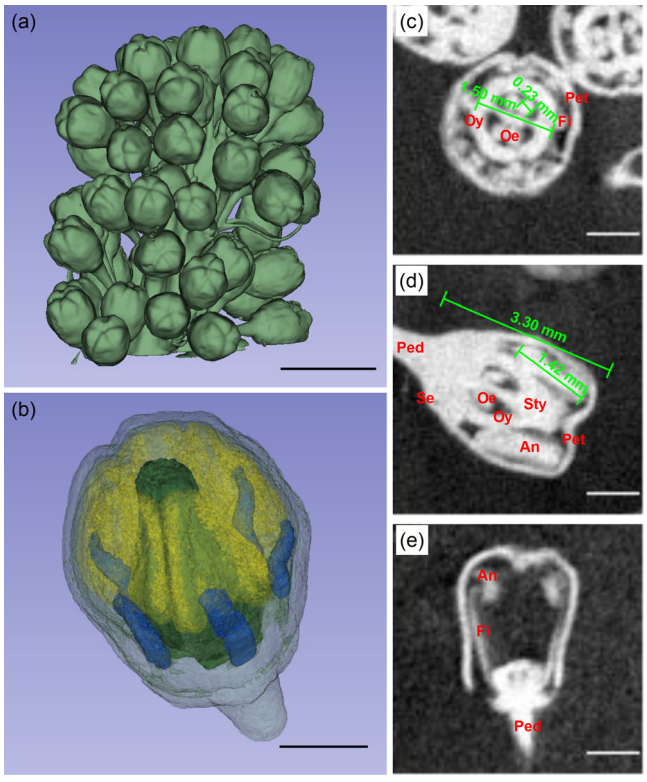

Figure 1. Micro-CT images of grapevine inflorescence and flowers: (a) 3D model with false colouring of the top part of an Isabella grapevine inflorescence; (a, b) 3D model of a single Isabella flower before anthesis showing anthers (yellow), filaments (blue), pistil (dark green) and calyptra (transparent); (c,d) virtual sections of reconstructed grapevine flowers micro-CT images of Isabella and Schwarzmann; and (e) before anthesis (light areas indicate organic matter and dark areas indicate voids). (c) View of the transverse-section of the inflorescence and measured morphometric parameters: ovary and ovule widths. (d, e) View of the longitudinal of the flowers and measured morphometric parameters; (d) flower and anther lengths. Scale bars are 5 mm in a and 1 mm in b–e. An, anther; Fi, filament; Oy, ovary; Oe, ovule; Ped, pedicel; Pet, petal; Se, sepal; Sty, style.

Table 1. Presence of voids in mature berries of Cabernet Sauvignon, Chambourcin, Flame Seedless, Isabella, Merlot, Sémillon, Shiraz and Sultana.

Cultivar	Firmness	DAF	TSS (°Brix)	Receptacle/berry junction	Brush region	Seed's ventral folds	Locule	Mesocarp	Total void volume (mm^3)	Void volume (% v/v)
Cabernet Sauvignon	Turgid	94	23.2 ± 0.8ab	2	4	4	2	0	2.69 ± 0.77	0.24 ± 0.05
Chambourcin	Turgid	98	18.4 ± 0.4c	3	4	2	3	0	5.99 ± 2.25	0.37 ± 0.12
Flame Seedless	Turgid	94	21.7 ± 1.0b	2	4	4	4	4	10.7 ± 2.38	0.36 ± 0.06
Isabella	Turgid	102	11.1 ± 0.9d	2	2	4	1	0	9.56 ± 0.72 (n = 3)	0.26 ± 0.01
Merlot	Turgid	99	24.1 ± 0.3a	1	4	4	3	0	8.07 ± 3.06	0.65 ± 0.24
Sémillon	Turgid	94	22.4 ± 0.3b	0	4	4	4	1	n.a.	n.a.
Shiraz	Turgid	94	22.9 ± 0.6b	2	4	4	4	0	6.32 ± 1.71 (n = 3)	0.41 ± 0.07
Shiraz	Shrivelled	94	25.5 ± 0.8a	2	4	4	4	0	3.93 ± 1.53 (n = 3)	0.73 ± 0.45
Sultana	Turgid	92	23.6 ± 0.7b	3	2	0	1	4	n.a.	n.a.

n = 4, unless otherwise noted; different lower-case letters indicate a statistical difference between cultivars with different firmness (one-way ANOVA, $P < 0.05$). There was no difference in total void volume or proportion of void volume between cultivars with different firmness. DAF, days after flowering; n.a., not applicable.

Figure 2. Reconstructed greyscale image of a longitudinal slice of a mature Muscat Gordo Blanco berry. Differences in density within the inner and outer regions of the pedicel, at the berry/pedicel junction, the 'detachment zone' within the brush, and around the seed are evident with dark grey areas representing greater air content. Low density lenticels are also visible. L, lenticels; P, pedicel; R, receptacle; VBP, peripheral vascular bundle; and VBO, ovular vascular bundle. Scale bar is 5 mm.

(Barthel 2006) in the Fiji software package (Schindelin et al. 2012). Differences in X-ray attenuation allowed the application of postprocessing thresholds to differentiate between void (black/dark area) and organic matter (pale grey/bright area). The 3D Slicer (ver. 4.10.2) (Fedorov et al. 2012) was used to generate 3D inflorescence and berry models. Total void volume was calculated in 3D Slicer. The proportion of void volume of total berry volume (% v/v) was also calculated.

Statistical analyses

GraphPad Prism 8 (GraphPad Software, San Diego, CA, USA) was used for all statistical analyses. One-way ANOVA was applied to TSS, total void volume and proportion of void volume.

Results

Flowers

Images of inflorescences and flower structures were obtained by micro-CT (Figure 1). The flower can be virtually sectioned at desired orientation to allow morphometric analysis of its components as illustrated in Figure 1a,b, including flower length, anther length, ovary width and ovule width. Ovules within the ovary were surrounded by voids (dark areas) (Figure 1a,b). Schwarzmann flowers contained only male flower parts (Figure 1c). Figure 1e depicts the components of a flower, including filament, anther and pistil artificially coloured.

Berries

Sampled between 92 and 102 DAF, berries of Merlot and visually shrivelled Shiraz had the highest TSS of 24.1 ± 0.3

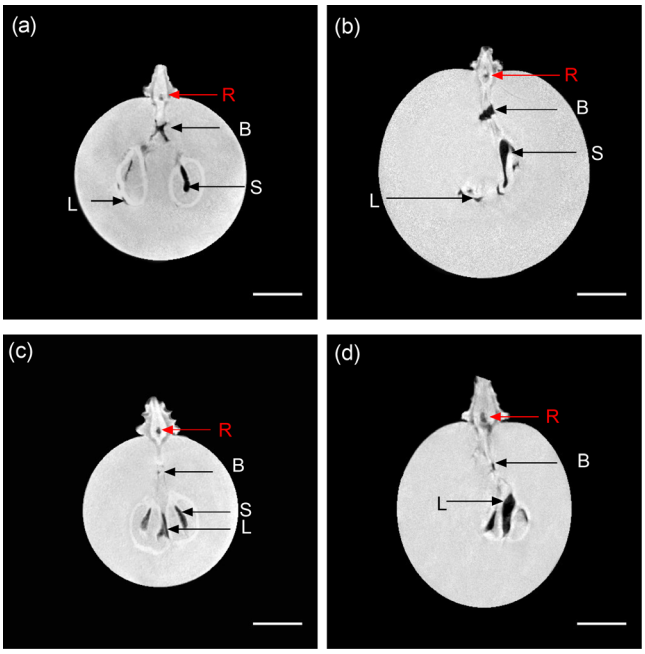

Figure 3. Reconstructed greyscale image of a longitudinal slice of mature grape berries depicting voids (light areas indicate organic matter and dark areas indicate voids). (a) Chambourcin; (b) Flame Seedless; (c) Merlot; and (d) Shiraz. Voids are present in the B, brush zone; L, locule; R, receptacle; and S, seed. Scale bars are 5 mm.

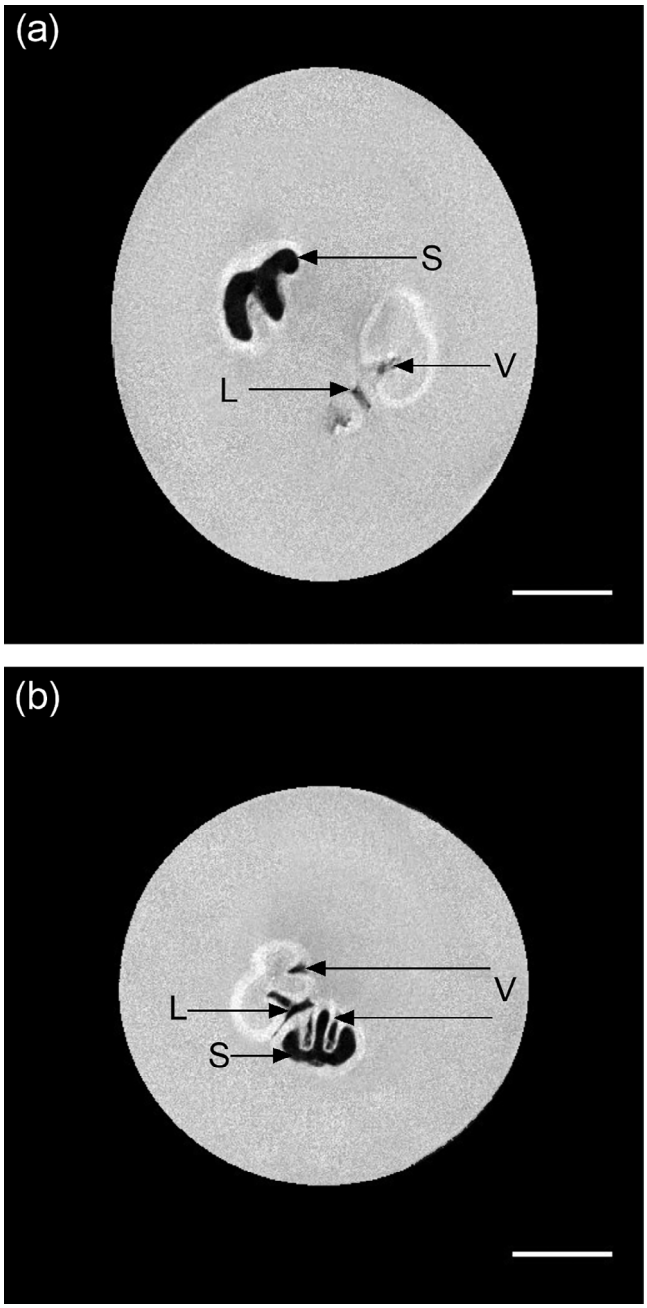

Figure 4. Transverse section through the equatorial region of mature berries. (a) Nyora, (b) Sémillon. Light areas indicate organic matter and dark areas indicate voids. L, void in locule; S, void within seed; and V, void in the seed's ventral folds. Scale bars are 5 mm.

and 25.5 ± 0.8°Brix, respectively. Turgid berries of Shiraz and all other *V. vinifera* cultivars were similar in sugar ripeness (21.7 ± 1.0 to 23.2 ± 0.8°Brix). Chambourcin and Isabella berries, however, had lower TSS of 18.4 ± 0.4 and 11.1 ± 0.9°Brix, respectively (Table 1). Reconstructed greyscale images of a longitudinal slice of a mature Muscat Gordo Blanco berry provides information on the positioning of the seeds, mesocarp, exocarp, receptacle and pedicel (Figure 2). Voids were evident in various regions of the fruit. These darker areas could be differentiated from organic matter, which was a pale grey (Figures 2 to 5). Longitudinal sections revealed variation in grayscale intensity between the interior (vascular region) and exterior (cortex) of the pedicel and receptacle of berries of all cultivars, thus suggesting that the exterior region proximal to the epidermis and lenticels could be porous (Figure 3). Voids were present in the pith of pedicels in some berries of each cultivar (Table 1). Void volume varied, with some of these quite prominent (Figure 3). The distal portion of the pedicel near the rachis junction did not show any such void.

A distinct void was evident between the hilum of the seeds and the brush region (i.e. confluence of peripheral and axial strands within the proximal mesocarp of the berry adjoining the receptacle that commonly detaches along with the receptacle under external force) in mature berries (Figures 3, 6) of all cultivars examined (Table 1). In Shiraz, these cavities were present in both turgid and slightly shrivelled berries (Figure 6c, Table 1).

The seeds were cuneate-shaped and enclosed by a prominent seed coat. Most seeds contained an embryo and endosperm; however, some were devoid of contents as evidenced by the black interior within the dense testa of the Nyora and Sémillon seeds (Figure 4, Table 1). Two fossettes, or ingrowths, were apparent on the ventral face of the seeds and these were often occupied by voids. Voids were also present between the seeds within the locules (Figures 3, 4, Table 1).

A significant number of macroscopic voids were present in the mesocarp of mature seedless berries, for example Flame Seedless and Sultana (Figures 5, 6a, b, Table 1). Of the seeded cultivars, only one cavity was evident near the epidermis of a Sémillon berry. No voids were observed around the stylar remnant. Across the cultivars (Table 1), total void volume (2.67 ± 0.77 to 10.7 ± 2.38 mm^3) and the proportion of void volume (0.24 ± 0.05 to 0.73 ± 0.45% v/v) within the berries did not differ despite differences in firmness.

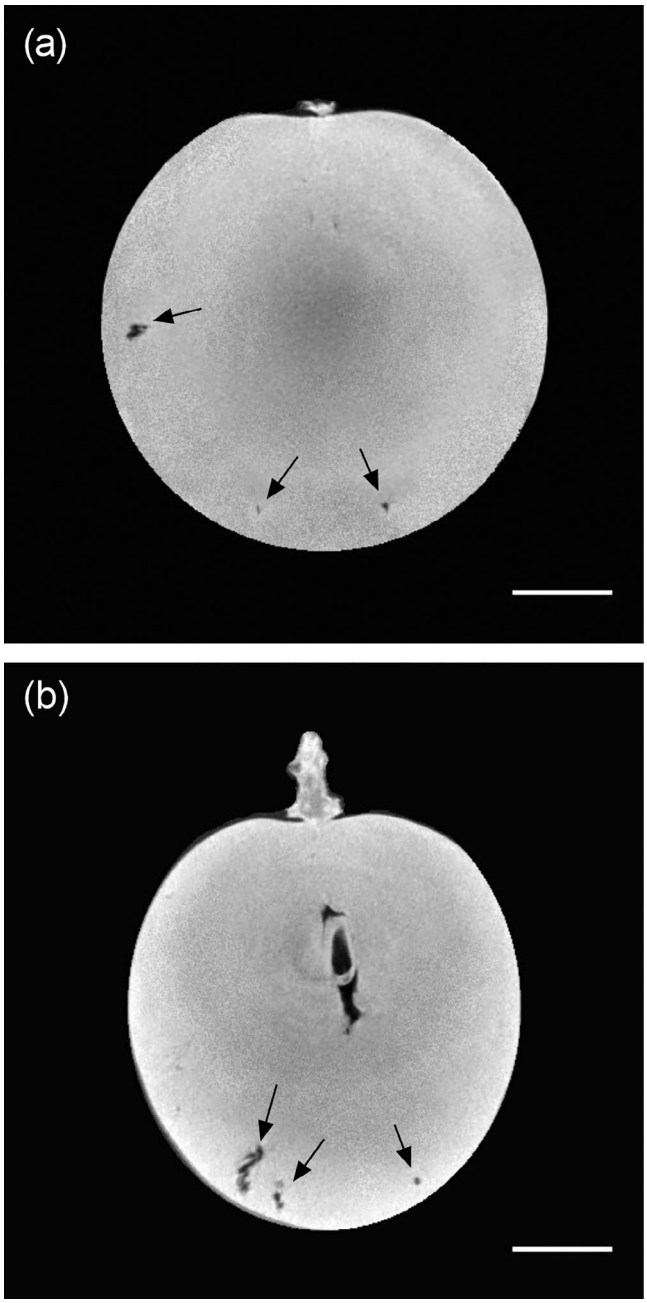

Figure 5. Longitudinal slice through the centre of the berry depicting peripheral voids within the mesocarp of mature tablegrape berries, indicated by black arrows. Light areas indicate organic matter and dark areas indicate voids. (a) Flame Seedless; and (b) Sultana. Scale bars are 5 mm.

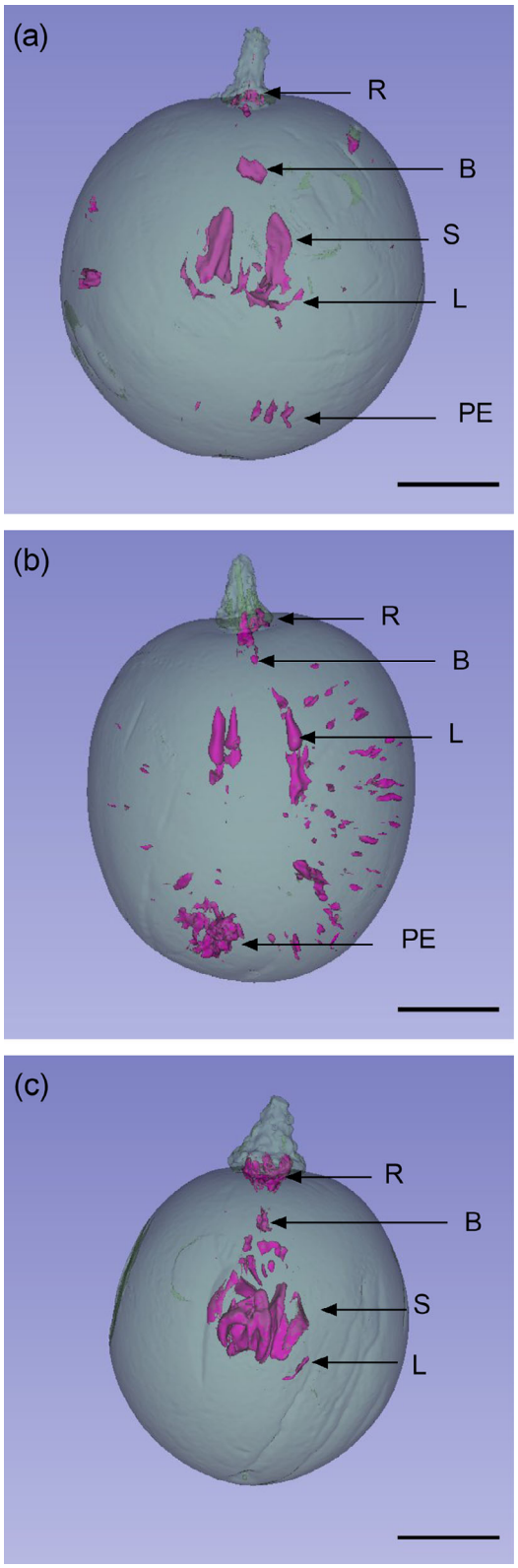

Figure 6. (a) Transparent 3D model, with false colouring, of grape berries showing voids (purple) in R, receptacle, B, brush region, S, seed's ventral folds, L, locule and PE, peripheral mesocarp region in Flame Seedless; (b) in the receptacle, brush, locule and peripheral mesocarp region in Sultana; and (c) in the receptacle, brush region, seed's ventral folds and locule in Shiraz. Scale bars are 5 mm.

Discussion

This micro-CT study has provided new insights into the structure of grapevine flowers and berries. With a scanning time of 14 min per specimen and minimal sample preparation, the spatial resolution of the micro-CT revealed detailed morphological features and quantitative information allowing length and volume calculation at the macroscale, using open source free software packages (ImageJ and 3D Slicer). We were able to map the spatial distribution of voids within in berries of different cultivars in vivo.

Voids were present in several regions of the berry including its pedicel. The diffuse intercellular air-filled network of the berry pedicel–receptacle was common across the eight cultivars imaged and confirmed previous results in Chardonnay (Xiao et al. 2018b). Most prominent in the external cortical region, this porous network likely aids in the passive diffusion and exchange of oxygen and carbon dioxide, as well as volatile organic compounds (VOCs) (Gil

et al. 2013), between the interior of the berry and the atmosphere. The exocarp of the grape berry is encased in a thick waxy cuticle with few lenticels leading to low gas permeability (Rogiers et al. 2004, 2005) thus entry points at the pedicel–receptacle may offer sufficient air exchange to maintain pericarp functionality. Indeed, artificial blockage of the pedicel–receptacle lenticels reduced berry internal oxygen concentration in the mesocarp of Chardonnay berries and resulted in ethanol accumulation and cell death (Xiao et al. 2018b). The lenticels on the berry pedicel thus likely play a significant part in respiratory gas transport, not only for delivering oxygen, but also for the removal of gases such as carbon dioxide and ethylene (Chervin et al. 2004, Sun et al. 2010).

An elliptical cavity was present in the pith of the pedicel at the receptacle/berry junction in some berries of most cultivars (Figure 3). It was segregated from the external regions of the receptacle and the berry mesocarp by what was likely a layer of liquid-filled vascular tissue. Knipfer et al. (2015b) also found air-filled spaces in the pith of grape berry receptacles of well-watered plants and therefore their occurrence does not appear to be related to water stress or desiccation. Because the void was not present in every berry of similar maturity, it may be due to some other environmental or physiological factors, and further work is required to shed more light on its occurrence.

Without the requirement for sectioning, micro-CT allowed visualisation of seed number and morphology, and the vascular traces leading to the hilum. Seed number influences final berry volume via growth regulator synthesis (Geelen et al. 1987, Cadot et al. 2006), yet there are few comprehensive descriptions of seed development in relation to grape berry development (Ristic and Iland 2005). It was not unusual to observe the pear-shaped seeds suspended within prominent hollow lumina of the locule. Seeds consume oxygen during development and the locular cavities may serve to avoid hypoxic conditions (Xiao et al. 2018b). The large voids at the most distal and proximal ends of the seeds and within the ventral folds may extend and connect with the porous network of the pedicel to supply the oxygen required to support seed growth and subsequent seed maturation. Additionally, micro-CT imaging revealed that at least one berry of most cultivars contained one or more 'empty' seeds (Figures 4b, 5, 6b). The integument was well developed, but the embryo and endosperm had undergone subsequent abortion (Pratt 1971, Ebadi et al. 1995). Both Flame Seedless and Sultana are stenospermocarpic where pollination and fertilisation occur but the embryo undergoes early abortion (Ramming et al. 2000). Of the two, only Flame Seedless had prominent locular lumina surrounding the seed traces, but this may be due to significantly smaller seed remnants of Sultana (Ramming et al. 2000).

A conspicuous void was present in the brush region, proximal to the seeds, herein, referred to as the 'detachment zone', in both mature turgid and shrivelled Shiraz berries, as well as all the other cultivars, including the seedless grapes. This 'detachment zone' may be related to berry abscission previously described at the proximal end of the berry for some cultivars at maturity (Fidelibus et al. 2007, Li et al. 2020). This zone comprised an irregular-shaped hollow structure, which was at times traversed with the vascular strands leading to the seeds. The cell separation and/or death process is regulated by endogenous and exogenous signals (Sawicki et al. 2015). Because this 'detachment zone' is localised, it is likely that programmed cell death is responsible, however, further evidence such as internucleosomal DNA fragmentation and chromatin condensation is required to confirm this. Reactive oxygen species formation, in association with ethylene and hypoxia, can induce cell death in several systems. All three of these components have been described during late ripening of grape berries (Tilbrook and Tyerman 2008, Pilati et al. 2014, Xiao et al. 2018b). The formation and progression of berry abscission has important practical and economic significance via consequences on the timing and ease of mechanical harvesting in vineyards. The estimated void volume (% v/v) of all cultivars was consistent with the locule relative volume previously found in Shiraz berries, also measured using micro-CT in combination with a pycnometry method (Xiao et al. 2018a). While the total void volume and the proportion of void volume to mesocarp volume within the berries did not differ between cultivars, the mesocarp of mature Sultana and Flame Seedless grapes was permeated with a network of prominent peripheral voids. None of the *V. vinifera* seeded grapes presented this feature despite similar maturity (number of days after flowering and TSS). The two seeded hybrids (Chambourcin and Isabella) also showed no peripheral voids. The peripheral cavities in Flame Seedless and Sultana berries were not likely the result of berry shrivelling and tissue collapse as, these two cultivars maintain their turgidity and firmness. Following on from our observations of voids in other berry parts, we suggest that these peripheral voids form a low resistance pathway for oxygen diffusion, and may also contribute to more effective gas exchange within the fruit interior (Ho et al. 2011). This conforms with the observation that seedless grapes show no or limited cell death during ripening (Tilbrook and Tyerman 2008, Fuentes et al. 2010). Gas conducting tissue within fruit may lead to a longer shelf life without the associated undesirable anaerobic metabolism. It is also likely that they play a role in tissue texture.

Conclusion

Micro-CT was found to be a rapid and informative, non-invasive technique to study the 3D structure of the reproductive organs of grapevines. It allowed for the visualisation of the porous nature of the receptacle region, the berry's internal 'detachment zone', and revealed that the mesocarp of seedless grape berries is permeated with voids. The preliminary data described here may provide a useful framework for the modelling of gas and VOCs diffusion through tissues. Further improvements in automated image processing should simplify data extraction. The detailed structural information provided by micro-CT may be overlaid with other functional, metabolic and genetic information, making it a desirable tool for integrated multidisciplinary research.

Acknowledgements

This research was conducted by the Australian Research Council Training Centre for Innovative Wine Production (www.arcwinecentre.org.au; project number IC170100008), funded by the Australian Government with additional support from Wine Australia, Waite Research Institute and industry partners. The University of Adelaide is a member of the Wine Innovation Cluster. The National Wine and Grape Industry Centre is an alliance between Charles Sturt University, New South Wales Department of Primary Industry, and the New South Wales Wine Industry Association. The authors acknowledge the facilities and scientific and technical assistance of the National Imaging Facility, a National

Collaborative Research Infrastructure Strategy (NCRIS) capability, at the Biomedical Magnetic Resonance Facility (BMRF), Western Sydney University.

References

Alba-Alejandre, I., Alba-Tercedor, J. and Vega, F.E. (2018) Observing the devastating coffee berry borer (*Hypothenemus hampei*) inside the coffee berry using micro-computed tomography. Scientific Reports **8**, 1–9.

Barthel, K.U. (2006) 3D-data representation with ImageJ. ImageJ user and developer conference; 18–19 May 2006; (CRP Henri Tudor: Luxembourg).

Boss, P.K., Buckeridge, E.J., Poole, A. and Thomas, M.R. (2003) New insights into grapevine flowering. Functional Plant Biology **30**, 593–606.

Brodersen, C.R., McElrone, A.J., Choat, B., Lee, E.F., Shacke, I.K.A. and Matthews, M.A. (2013) In vivo visualizations of drought-induced embolism spread in *Vitis vinifera*. Plant Physiology **161**, 1820–1829.

Brodersen, C.R., Lee, E.F., Choat, B., Jansen, S., Phillips, R.J., Shackel, K.A., McElrone, A.J. and Matthews, M.A. (2011) Automated analysis of three-dimensional xylem networks using high-resolution computed tomography. New Phytologist **191**, 1168–1179.

Cadot, Y., Miñana-Castelló, M.T. and Chevalier, M. (2006) Anatomical, histological, and histochemical changes in grape seeds from *Vitis vinifera* L. cv Cabernet franc during fruit development. Journal of Agricultural and Food Chemistry **54**, 9206–9215.

Chervin, C., El-Kereamy, A., Roustan, J.-P., Latché, A., Lamon, J. and Bouzayen, M. (2004) Ethylene seems required for the berry development and ripening in grape, a non-climacteric fruit. Plant Science **167**, 1301–1305.

Cochard, H., Delzon, S. and Badel, E. (2015) X-ray microtomography (micro-CT): a reference technology for high-resolution quantification of xylem embolism in trees. Plant, Cell & Environment **38**, 201–206.

Dean, R., Bobek, G., Stait-Gardner, T., Clarke, S.J., Rogiers, S.Y. and Price, W.S. (2016) Time-course study of grape berry split using diffusion magnetic resonance imaging. Australian Journal of Grape and Wine Research **22**, 240–244.

Dean, R.J., Stait-Gardner, T., Clarke, S.J., Rogiers, S.Y., Bobek, G. and Price, W.S. (2014) Use of diffusion magnetic resonance imaging to correlate the developmental changes in grape berry tissue structure with water diffusion patterns. Plant Methods **10**, 35.

du Plessis, A. and Broeckhoven, C. (2019) Looking deep into nature: a review of micro-computed tomography in biomimicry. Acta Biomaterialia **85**, 27–40.

Ebadi, A., Coombe, B.G. and May, P. (1995) Fruit-set on small Chardonnay and Shiraz vines grown under varying temperature regimes between budburst and flowering. Australian Journal of Grape and Wine Research **1**, 3–10.

Fedorov, A., Beichel, R., Kalpathy-Cramer, J., Finet, J., Fillion-Robin, J.-C., Pujol, S., Bauer, C., Jennings, D., Fennessy, F. and Sonka, M. (2012) 3D slicer as an image computing platform for the quantitative imaging network. Magnetic Resonance Imaging **30**, 1323–1341.

Fidelibus, M.W., Cathline, K.A. and Burns, J.K. (2007) Potential abscission agents for raisin, table, and wine grapes. HortScience **42**, 1626–1630.

Fuentes, S., Sullivan, W., Tilbrook, J. and Tyerman, S. (2010) A novel analysis of grapevine berry tissue demonstrates a variety-dependent correlation between tissue vitality and berry shrivel. Australian Journal of Grape and Wine Research **16**, 327–336.

Gargiulo, L., Grimberg, Å., Repo-Carrasco-Valencia, R., Carlsson, A. S. and Mele, G. (2019) Morpho-densitometric traits for quinoa (*Chenopodium quinoa* Willd.) seed phenotyping by two X-ray micro-CT scanning approaches. Journal of Cereal Science **90**, 102829.

Geelen, T., Varga, A. and Bruinsma, J. (1987) Cell division and elongation in the exocarp of tomato fruits grown in systems *in vitro* and on the vine. Journal of Plant Physiology **130**, 343–349.

Gil, M., Bottini, R., Berli, F., Pontin, M., Silva, M.F. and Piccoli, P. (2013) Volatile organic compounds characterized from grapevine (*Vitis vinifera* L. cv. Malbec) berries increase at pre-harvest and in response to UV-B radiation. Phytochemistry **96**, 148–157.

Hardie, W.J., O'Brien, T. and Jaudzems, V. (1996) Morphology, anatomy and development of the pericarp after anthesis in grape, *Vitis vinifera* L. Australian Journal of Grape and Wine Research **2**, 97–142.

Heeraman, D.A., Hopmans, J.W. and Clausnitzer, V. (1997) Three dimensional imaging of plant roots in situ with X-ray computed tomography. Plant and Soil **189**, 167–179.

Herremans, E., Verboven, P., Verlinden, B.E., Cantre, D., Abera, M., Wevers, M. and Nicolaï, B.M. (2015) Automatic analysis of the 3-D microstructure of fruit parenchyma tissue using X-ray micro-CT explains differences in aeration. BMC Plant Biology **15**, 264.

Ho, Q.T., Verboven, P., Verlinden, B.E., Herremans, E., Wevers, M., Carmeliet, J. and Nicolaï, B.M. (2011) A three-dimensional multi-scale model for gas exchange in fruit. Plant Physiology **155**, 1158–1168.

Hubeau, M. and Steppe, K. (2015) Plant-PET scans: in vivo mapping of xylem and phloem functioning. Trends in Plant Science **20**, 676–685.

Knipfer, T., Eustis, A., Brodersen, C., Walker, A.M. and McElrone, A.J. (2015a) Grapevine species from varied native habitats exhibit differences in embolism formation/repair associated with leaf gas exchange and root pressure. Plant, Cell & Environment **38**, 1503–1513.

Knipfer, T., Fei, J., Gambetta, G.A., McElrone, A.J., Shackel, K.A. and Matthews, M.A. (2015b) Water transport properties of the grape pedicel during fruit development: insights into xylem anatomy and function using microtomography. Plant Physiology **168**, 1590–1602.

Kuhn, N., Guan, L., Dai, Z.W., Wu, B.-H., Lauvergeat, V., Gomès, E., Li, S.-H., Godoy, F., Arce-Johnson, P. and Delrot, S. (2013) Berry ripening: recently heard through the grapevine. Journal of Experimental Botany **65**, 4543–4559.

Li, M., Huang, Z., You, X., Zhang, Y., Wei, P., Zhou, K. and Wang, Y. (2020) Relationships between cell structure alterations and berry abscission in table grapes. Frontiers in Nutrition **7**, 69.

Li, M., Klein, L.L., Duncan, K.E., Jiang, N., Chitwood, D.H., Londo, J.P., Miller, A.J. and Topp, C.N. (2019) Characterizing 3D inflorescence architecture in grapevine using X-ray imaging and advanced morphometrics: implications for understanding cluster density. Journal of Experimental Botany **70**, 6261–6276.

May, P. (2000) From bud to berry, with special reference to inflorescence and bunch morphology in *Vitis vinifera* L. Australian Journal of Grape and Wine Research **6**, 82–98.

Nunan, K.J., Sims, I.M., Bacic, A., Robinson, S.P. and Fincher, G.B. (1998) Changes in cell wall composition during ripening of grape berries. Plant Physiology **118**, 783–792.

Pierantoni, M., Tenne, R., Brumfeld, V., Kiss, V., Oron, D., Addadi, L. and Weiner, S. (2017) Plants and light manipulation: the integrated mineral system in okra leaves. Advanced Science **4**, 1600416.

Pilati, S., Brazzale, D., Guella, G., Milli, A., Ruberti, C., Biasioli, F., Zottini, M. and Moser, C. (2014) The onset of grapevine berry ripening is characterized by ROS accumulation and lipoxygenase-mediated membrane peroxidation in the skin. BMC Plant Biology **14**, 87.

Pratt, C. (1971) Reproductive anatomy in cultivated grapes-a review. American Journal of Enology and Viticulture **22**, 92–109.

Ramming, D.W., Emershad, R.L. and Tarailo, R. (2000) A stenospermocarpic, seedless *Vitis vinifera*×*Vitis rotundifolia* hybrid developed by embryo rescue. HortScience **35**, 732–734.

Ristic, R. and Iland, P.G. (2005) Relationships between seed and berry development of *Vitis vinifera* L. cv Shiraz: developmental changes in seed morphology and phenolic composition. Australian Journal of Grape and Wine Research **11**, 43–58.

Rogiers, S.Y., Hatfield, J.M., Jaudzems, V.G., White, R.G. and Keller, M. (2004) Grape berry cv. Shiraz epicuticular wax and transpiration during ripening and preharvest weight loss. American Journal of Enology and Viticulture **55**, 121–127.

Rogiers, S.Y., Whitelaw-Weckert, M., Radovanonic-Tesic, M., Greer, L.A., White, R. and Steel, C.C. (2005) Effects of spray adjuvants on grape (*Vitis vinifera*) berry microflora, epicuticular wax and susceptibility to infection by *Botrytis cinerea*. Australasian Plant Pathology **34**, 221–228.

Sawicki, M., Aït Barka, E., Clément, C., Vaillant-Gaveau, N. and Jacquard, C. (2015) Cross-talk between environmental stresses and plant metabolism during reproductive organ abscission. Journal of Experimental Botany **66**, 1707–1719.

Schindelin, J., Arganda-Carreras, I., Frise, E., Kaynig, V., Longair, M., Pietzsch, T., Preibisch, S., Rueden, C., Saalfeld, S. and Schmid, B. (2012) Fiji: an open-source platform for biological-image analysis. Nature Methods **9**, 676–682.

Shavrukov, Y.N., Dry, I.B. and Thomas, M.R. (2004) Inflorescence and bunch architecture development in *Vitis vinifera* L. Australian Journal of Grape and Wine Research **10**, 116–124.

Signorelli, S., Shaw, J., Hermawaty, D., Wang, Z., Verboven, P., Considine, J.A. and Considine, M.J. (2020) The initiation of bud burst in grapevine features dynamic regulation of the apoplastic pore size. Journal of Experimental Botany **71**, 719–729.

Srinivasan, C. and Mullins, M.G. (1976) Reproductive anatomy of the grape-vine (*Vitis vinifera* L.): origin and development of the anlage and its derivatives. Annals of Botany **40**, 1079–1084.

Srinivasan, C. and Mullins, M.G. (1981) Physiology of flowering in the grapevine—a review. American Journal of Enology and Viticulture **32**, 47–63.

Staedler, Y.M., Masson, D. and Schönenberger, J. (2013) Plant tissues in 3D via X-ray tomography: simple contrasting methods allow high resolution imaging. PLoS One **8**, e75295.

Sun, L., Zhang, M., Ren, J., Qi, J., Zhang, G. and Leng, P. (2010) Reciprocity between abscisic acid and ethylene at the onset of berry ripening and after harvest. BMC Plant Biology **10**, 257.

Tilbrook, J. and Tyerman, S.D. (2008) Cell death in grape berries: varietal differences linked to xylem pressure and berry weight loss. Functional Plant Biology **35**, 173–184.

Tracy, S.R., Roberts, J.A., Black, C.R., McNeill, A., Davidson, R. and Mooney, S.J. (2010) The X-factor: visualizing undisturbed root architecture in soils using X-ray computed tomography. Journal of Experimental Botany **61**, 311–313.

Verboven, P., Herremans, E., Helfen, L., Ho, Q.T., Abera, M., Baumbach, T., Wevers, M. and Nicolaï, B.M. (2015) Synchrotron X-ray computed laminography of the three-dimensional anatomy of tomato leaves. The Plant Journal **81**, 169–182.

Wang, C.-N., Hsu, H.-C., Wang, C.-C., Lee, T.-K. and Kuo, Y.-F. (2015) Quantifying floral shape variation in 3D using micro-computed tomography: a case study of a hybrid line between actinomorphic and zygomorphic flowers. Frontiers in Plant Science **6**, 724.

Wang, Z., Verboven, P. and Nicolai, B. (2017) Contrast-enhanced 3D micro-CT of plant tissues using different impregnation techniques. Plant Methods **13**, 105.

Wason, J.W., Huggett, B.A. and Brodersen, C.R. (2017) MicroCT imaging as a tool to study vessel endings in situ. American Journal of Botany **104**, 1424–1430.

Xiao, Z., Liao, S., Rogiers, S., Sadras, V.O. and Tyerman, S. (2018a) Effect of water stress and elevated temperature on hypoxia and cell death in the mesocarp of Shiraz berries. Australian Journal of Grape and Wine Research **24**, 487–497.

Xiao, Z., Rogiers, S.Y., Sadras, V.O. and Tyerman, S.D. (2018b) Hypoxia in grape berries: the role of seed respiration and lenticels on the berry pedicel and the possible link to cell death. Journal of Experimental Botany **69**, 2071–2083.

Manuscript received: 8 August 2020
Revised manuscript received: 12 November 2020
Accepted: 14 November 2020